ARTICLE

OPEN

Organic semiconductor density of states controls the energy level alignment at electrode interfaces

Martin Oehzelt[1,2], Norbert Koch[1,2] & Georg Heimel[2]

Minimizing charge carrier injection barriers and extraction losses at interfaces between organic semiconductors and metallic electrodes is critical for optimizing the performance of organic (opto-) electronic devices. Here, we implement a detailed electrostatic model, capable of reproducing the alignment between the electrode Fermi energy and the transport states in the organic semiconductor both qualitatively and quantitatively. Covering the full phenomenological range of interfacial energy level alignment regimes within a single, consistent framework and continuously connecting the limiting cases described by previously proposed models allows us to resolve conflicting views in the literature. Our results highlight the density of states in the organic semiconductor as a key factor. Its shape and, in particular, the energy distribution of electronic states tailing into the fundamental gap is found to determine both the minimum value of practically achievable injection barriers as well as their spatial profile, ranging from abrupt interface dipoles to extended band-bending regions.

---

[1] Helmholtz-Zentrum Berlin für Materialien und Energie GmbH, Bereich Solarenergieforschung, Albert-Einstein-Straße 15, 12489 Berlin, Germany. [2] Institut für Physik, Humboldt-Universität zu Berlin, Newtonstraße 15, 12489 Berlin, Germany. Correspondence and requests for materials should be addressed to M.O. (email: martin.oehzelt@helmholtz-berlin.de).

Organic electronics has tremendous potential for extending and complementing the range of conventional semiconductor applications and has, to some extent, already entered the market. This is especially true for organic light-emitting diodes (OLEDs)[1–6] in displays of mobile devices and, very recently, in television panels. In the fields of solid state lighting, integrated circuits based on organic field-effect transistors (OFETs)[7–11] and organic photovoltaic cells (OPVCs)[12–16], commercial breakthrough is still ahead, with considerable effort in fundamental as well as applied research currently undertaken. All these devices have in common one or more organic semiconductor layer(s), possessing (as every semiconductor) a non-vanishing energy gap between occupied and empty electronic states. Electrical connection of the organic semiconductor(s) to peripheral circuitry, however, must inevitably be realized by metallic contacts, with a wide range of elemental metals and degenerately doped inorganic or organic semiconductors employed today[3,16,17]. These are characterized by a continuum of electronic states filled up to a common electron chemical potential, often referred to as the Fermi level, E_F. Depending on the intended function of the organic electronic device, charges must either be injected from the metallic electrode into the organic semiconductor (OLED/OFET) or they must be collected from the organic semiconductor by the metallic electrode (OPVC)[18,19].

In Fig. 1a, a typical situation for the energetic alignment of all relevant electronic states is sketched schematically. We immediately realize that, in such a situation, charge carriers encounter energy barriers, Δ_e for electrons and Δ_h for holes, if they are to be injected and that, for their extraction, corresponding energy losses occur. This has led the community to acknowledge that minimizing these barriers/losses and, in a broader sense, controlling interfacial energy level alignment in general, is a key factor for improving device performance[18,20–29].

If, for a specific material pair, the situation sketched in Fig. 1a is found unsatisfactory, the obvious strategy is to reduce barriers/losses by either moving E_F towards the occupied or unoccupied molecular levels (for example, by modifying the electrode work function or by choosing a different electrode material) or to move one of the molecular levels closer to E_F (typically by choosing a different organic semiconductor).

As the ultimate limit of such a strategy, one could assume that it was possible to eliminate barriers/losses altogether (Fig. 1b). In practice, however, this was only observed for monolayers of select molecules[30–34], but could never be achieved for multilayer organic semiconductor films of device-relevant thickness. There, in contrast, non-vanishing energy barriers were found to remain (Fig. 1c). Several models have been developed in the past to explain this phenomenon[20–29,35–41], each of which will be discussed to some detail in corresponding sections below. They differ not only in their intended range of applicability (from a single organic semiconductor layer[26] to thick films[23,25,27,29]) but also in the envisioned regimes of electronic coupling strength between organic and electrode (from weak coupling with a passivated electrode[23,25,27,29] to intermediate coupling with an atomically clean metal[26]) as well as in the assumed energy distribution of the electronic states in the organic (from discrete[23,25,29] to continuous[26,27]).

Here, we present results from a numerical electrostatic model, which allows treating all these various scenarios on equal footing. The full wealth of all encountered interfacial phenomena is described qualitatively and, provided required input data are available, even quantitatively[24]. With previous models naturally emerging as different limiting cases, we consolidate diverging views in literature regarding the physical origin of non-vanishing injection barriers (Fermi level pinning by metal-induced density of gap states[26] versus finite-temperature occupation of discrete molecular levels[23,25]) as well as their spatial profile (interface dipole[26,29] versus band bending[25,27]), and we provide a single, coherent framework for understanding the energy level alignment at interfaces between metallic electrodes and organic semiconductors.
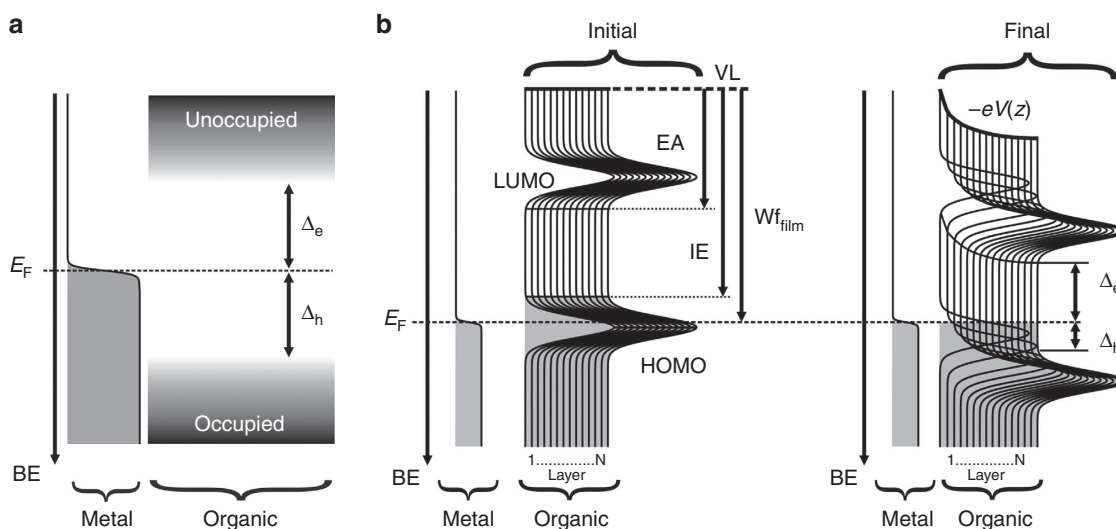
Figure 1 | Sketch of the energy level alignment at organic/electrode interfaces. (**a**) Schematic showing the Fermi-Dirac occupation function with Fermi level E_F for the metallic side of the interface. The difference in binding energy (BE) between E_F and the onsets of occupied and unoccupied density of states (DOS) on the organic semiconductor side are the charge injection barriers, Δ_h for holes and Δ_e for electrons, respectively. (**b**) Example of a possible initial situation for the iterative electrostatic model described in the text. The energy differences between the onsets of the DOS derived from the highest occupied molecular orbitals (HOMOs) and the lowest unoccupied molecular orbitals (LUMOs) to the vacuum level (VL) define the ionization energy (IE) and the electron affinity (EA) of the organic semiconductor, respectively. The energy difference between E_F and VL is the work function of the organic film (Wf$_{film}$). (**c**) Final energy level alignment after convergence of the iterative scheme discussed in the text. With increasing distance z from the electrode, the DOS increasingly shifts to higher BE by the local electron potential energy $-eV(z)$, thus increasing Δ_h and decreasing Δ_e with respect to the initial situation.

Results

Introducing the model. Our model is inspired by the earlier work of Vasquez *et al.*[26,39] and, more recently, of Blakesley *et al.*[27,28], as well as of Greiner *et al.*[23] and Ley *et al.*[25] Going beyond refs 23,25, however, we take into account a continuous density of states (DOS) both for the occupied and the unoccupied levels in the organic semiconductor. For simplicity, we start with the common choice[27,42,43] of one Gaussian peak, $G(E - E_H, \sigma_H)$, arising from the energy distribution of the highest occupied molecular orbitals (HOMOs) and one, $G(E - E_L, \sigma_L)$, from the distribution of the lowest unoccupied molecular orbitals (LUMOs) as indicated in Fig. 1b. To unambiguously define these peaks, both the energies of their maxima, E_H and E_L, and their standard deviations, σ_H and σ_L, need to be specified. The latter can be approximated, for example, by the width of the HOMO-derived feature observed in ultraviolet photoelectron spectroscopy (UPS). Here, we adapt the constant value of $\sigma_H = \sigma_L = 0.25$ eV, found for the archetypical organic semiconductor pentacene[44]. From UPS and inverse photoelectron spectroscopy also the ionization energy (IE = 4.8 eV)[44] and the electron affinity (EA = 2.6 eV)[45] of pentacene are known. These quantities are typically determined from the energy difference between the vacuum level (VL) and the low-binding energy onset of the UPS spectrum and the high-binding energy onset of the inverse photoelectron spectroscopy spectrum, respectively. Choosing the onset of a Gaussian peak to be the energy, where the tangent through the inflection point crosses the base line, puts the peak centres 2σ away from the so obtained onsets, that is, at $E_H = 5.3$ eV and $E_L = 2.1$ eV, respectively. Also indicated in Fig. 1b is the work function, Wf_{film}, given by the energy difference between the Fermi level and the VL outside the organic semiconductor film. Note that, in the specific situation shown, Wf_{film} is actually higher than the IE of the organic semiconductor, where electrons reside at energies above E_F before charge equilibration. It is, therefore, clear that in the course of establishing a common electron chemical potential, charge will flow across the interface. To quantify the amount of transferred charge in the general case, we discretize the organic semiconductor film into layers of thickness Δz and distance z from the electrode surface. We then calculate the charge density $\rho(z)$ in each of these layers by integrating

$$
\rho(z) = e \cdot n \cdot \left\{ \int_{-\infty}^{+\infty} dE \cdot f_H(E) \cdot D_H[E + eV(z)] \right.
$$
$$
\left. - \int_{-\infty}^{+\infty} dE \cdot f_L(E) \cdot D_L[E + eV(z)] \right\} \quad (1)
$$

with e the (positive) elementary charge, n the number of molecules per unit area and per discretization interval Δz. As the IE and EA values reported above pertain to pentacene molecules 'standing' on the electrode with their long molecular axes almost parallel to the surface normal[44,45], we accordingly choose $\Delta z = 1.42$ nm, the distance d_{001} between the crystallographic (001) planes in the pentacene single crystal[46]; Δz then corresponds to the height of one molecular layer. For the sake of simplicity, we consider layer-by-layer growth of pentacene only, with $n = 4.1 \times 10^{18}$ molecules/(m$^2 \cdot \Delta z$). Note, however, that fractional coverages and different growth modes could easily be incorporated by accordingly choosing layer-specific values for n.

The first integral in the curly brackets of equation (1) yields the number of holes in the occupied DOS of the organic semiconductor and the second integral the number of electrons in the unoccupied DOS. While of noticeable consequence only for highly degenerate systems, we, nevertheless, follow refs 23,25 by

allowing, in contrast to refs 27,28, only single charging of each molecule, which slightly modifies the Fermi function for each individual energy level under consideration to

$$
f_H(E) = \frac{1}{\frac{1}{g_H} e^{-\beta(E - E_F)} + 1},
$$
$$
f_L(E) = \frac{1}{\frac{1}{g_L} e^{+\beta(E - E_F)} + 1}. \quad (2)
$$

Here, g_H and g_L are the HOMO and LUMO (spin-) degeneracies, both 2 in the case of pentacene, and $\beta = 1/k_B T$ with k_B the Boltzmann constant and T the temperature, set to 300 K throughout the paper. Finally, the energy distributions of HOMO- and LUMO-derived levels are $D_H[E + eV(z)] = G[E - E_H + eV(z), \sigma_H]$ and $D_L[E + eV(z)] = G[E - E_L + eV(z), \sigma_L]$ in our model case, unless otherwise noted. We stress, however, that (i) any peak shape can be used instead of a Gaussian, (ii) each discretization interval could have a different DOS to account, for example, for image-charge screening by the metal, (iii) more molecular states can easily be taken into account by adding the respective terms in the curly brackets and (iv) potential temperature effects can be included in the standard deviation $\sigma = \sigma(T)$; for the values used here, $2\sigma = 0.50$ eV is about 20 times bigger than $k_B T$ at $T = 300$ K and, therefore, the temperature dependence of $f_{H/L}(E)$ has only little impact on level alignment.

Finally, the electrostatic potential across the organic semiconductor film, $V(z)$, is first set to zero for calculating an initial guess of the charge density via equation (1). Once known, this $\rho(z)$ serves to find the next $V(z)$, which, going beyond refs 23,25, we obtain by numerically solving the generalized one-dimensional Poisson equation

$$
\nabla[\varepsilon(z)\nabla V(z)] = -\frac{\rho(z)}{\varepsilon_0} \quad (3)
$$

with the discrete-difference method on a variable grid, using the second-order, central-difference scheme with mixed Dirichlet $[V(0) = 0]$ and von Neumann $[V'(d) = 0]$ boundary conditions, where d is the total thickness of the considered organic film and ε_0 the vacuum permittivity. For our first illustrative case of a homogenous pentacene film, we assume a static dielectric constant ε of ~ 3.6, as recently determined by impedance measurements[47]; note, however, that each discretization interval could, in principle, also be given a different dielectric constant. The DOS of each discretization interval is then shifted in energy by the respective $-eV(z)$, as shown in Fig. 1c, and the next $\rho(z)$ is again generated by occupying all states in the organic up to E_F. This self-consistent process is iterated until the difference in charge density between cycles is less than one electron per layer and square meter and the final injection barriers are obtained as $\Delta_e = E_F - EA$ and $\Delta_h = IE - E_F$.

Some illustrative results. To illustrate the results delivered by the method just described, we first consider 20 layers (~ 30 nm) of standing pentacene with E_F set to lie right at the energy of the HOMO peak maximum. The self-consistent solution of the Poisson equation for this situation is depicted in Fig. 2a,b, showing the charge density and the electron potential energy, respectively. The charge density rapidly vanishes with increasing distance from the electrode surface and reaches almost zero at 5 nm. The corresponding potential energy, which locally shifts HOMO, LUMO and VL by the same amount (IE and EA remain constant), is characteristic for band bending—a term somewhat liberally borrowed from inorganic semiconductor physics despite the fundamental difference that, instead of actual bands there, a distribution of localized states is assumed here. Although this phenomenon has often been attributed to (impurity or

3

intentional) doping[29,48,49] in the past, it has recently been argued to arise also in intrinsic organic semiconductors, both of the conjugated-polymer[27] and the small-molecule variety[24,25]. In trying to relate our results to experimental observations, it is important to recall that the work function measured by, for example, UPS or Kelvin probe only reveals the electron potential energy $-eV(z \geq d)$ just outside the organic film (highlighted in Fig. 2b). As pointed out in refs 50–53, however, the sequence of $-eV(d)$ values obtained by increasing the total thickness d of an organic film in a step-wise manner and probing the surface potential at each step does not, in fact, recover the electron potential energy profile $-eV(z)$ within the organic film for any thickness (Fig. 2c).

Fermi level pinning. With this in mind, we now plot in Fig. 3a the total potential energy change, $-eV(d)$, across pentacene films of increasing d, for a series of different Fermi level energies. Clearly, when E_F lies around mid-gap of the organic semiconductor, only very little charge is transferred from/to the metal electrode and, consequently, the potential energy profile remains close to flat. Upon E_F approaching either the HOMO or the LUMO levels, however, pronounced charge transfer and, accordingly, ever higher and steeper potential energy changes across the organic film are obtained. Practically, the Fermi level is

shifted by choosing electrodes of different work function, Wf_{elec}, defined by the energy difference between E_F and the VL just above the bare electrode surface with no organic material present. The energy barriers/losses for charge carriers, Δ_e and Δ_h, are then related to Wf_{elec} and $-eV(d)$ through

$$\Delta_e = [Wf_{elec} + ID - eV(d)] - EA, \quad (4)$$

$$\Delta_h = IE - [Wf_{elec} + ID - eV(d)], \quad (5)$$

where ID is the interface dipole. Either because of contamination through atmospheric and/or solvent exposure or owing to deliberate passivation with inert buffer layers, the ID is often found to be (close to) zero for practically employed electrodes in organic electronics. However, microscopic charge rearrangements originating in a variety of physical and/or chemical phenomena occurring between the electrode surface and the first organic layer can, in general, lead to appreciable IDs[22,37,38,54–56]. If available, for example, through a fully atomistic and quantum-mechanical treatment on a particular system, then they can, of course, be readily incorporated into the present model through equations (4) and (5). To study the impact of Wf_{elec} on $\Delta_{e/h}$ on more general grounds, however, we refer to an effective electrode work function

$$\Phi_{eff} = Wf_{elec} + ID, \quad (6)$$
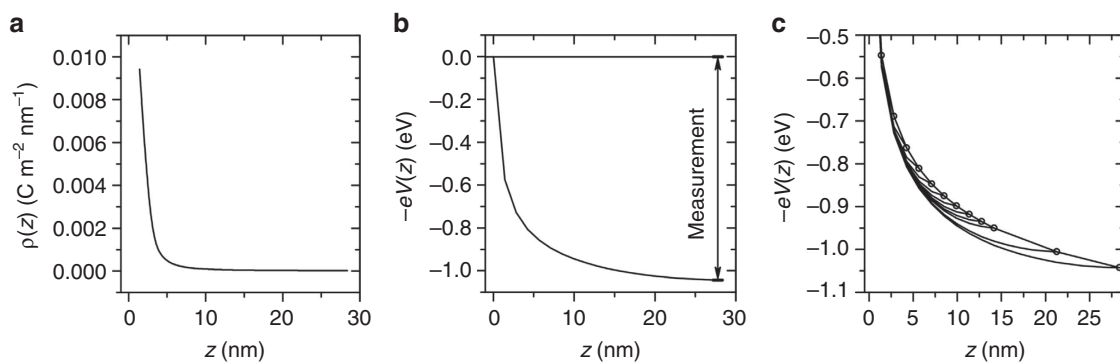
Figure 2 | Exemplary results of the iterative electrostatic model. (**a**) Calculated charge density $\rho(z)$, and (**b**) electron potential energy $-eV(z)$ within a $d = 30$ nm thick (≈ 20 layer) pentacene film. Surface sensitive experimental methods (for example, UPS or Kelvin probe) only determine the total electron potential energy drop $-eV(d)$ across the entire organic-semiconductor film. (**c**) $-eV(z)$ for a range of different film thicknesses d up to 30 nm, highlighting that the series of experimentally determined $-eV(d)$, shown as line connecting open circles, does not reproduce the band-bending $-eV(z)$ within the organic semiconductor for any thickness.
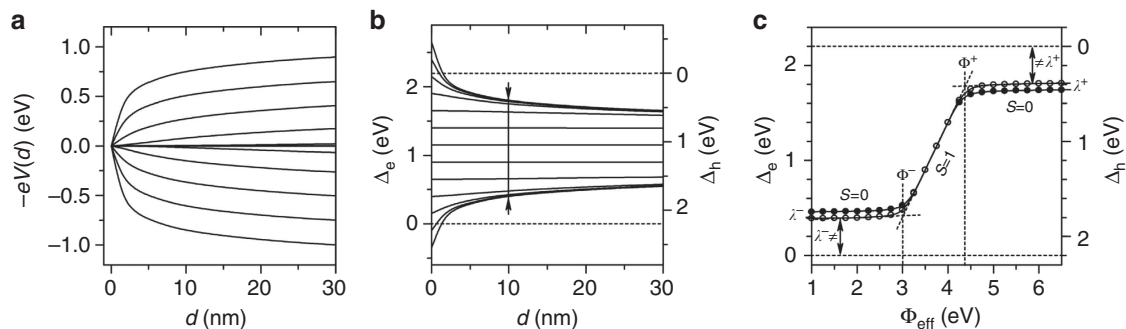
Figure 3 | Impact of effective substrate work function on band bending and barriers. (**a**) Total electron potential energy change $-eV(d)$ across pentacene films of varying thickness d for a series of Fermi level energies ranging from 0.15 eV below E_L, the initial LUMO peak energy (top trace), to 0.05 eV above E_H, the initial HOMO peak energy (bottom trace). (**b**) Data from **a** converted to injection barriers Δ_e for electrons (left axis) and Δ_h for holes (right axis). Dashed horizontal lines indicate respective values of zero and the vertical line highlights the cut visualized in **c**. (**c**) Injection barriers Δ_e (left axis) and Δ_h (right axis) as a function of effective substrate work function Φ_{eff} for a $d = 10$ nm thick pentacene film with (●) and without (○) polaronic relaxation energies λ^+ (for holes) and λ^- (for electrons) taken into account. The transitions between the regions with slope $S = 0$ and $S = 1$ mark the so-called pinning work functions, Φ^- for LUMO pinning and Φ^+ for HOMO pinning. The lowest achievable injection barriers are not related to $\lambda^{+/-}$.

in the following. Before charge equilibration, that is, with $V(d) = 0$, the initial barriers are then simply given by $\Delta_e = \Phi_{eff} - EA$ and $\Delta_h = IE - \Phi_{eff}$, respectively.

This now allows us to make the transition from relative potential energy changes for different values of E_F (Fig. 3a) to absolute values of Δ_e and Δ_h for a series of effective electrode work functions, both of which are now quantities readily accessible through experiment. Figure 3b illustrates that changing Φ_{eff} indeed permits tuning the interfacial energy barriers/losses, but only within a certain range. For our model case of pentacene, the achievable minimum separation between E_F and EA/IE rapidly converges to $\Delta_e = \Delta_h = 0.4\,eV$ with increasing film thickness, where decreasing Φ_{eff} below $\sim 3.0\,eV$ does not further reduce Δ_e and increasing Φ_{eff} beyond $\sim 4.4\,eV$ does not further reduce Δ_h. A more convenient way of visualizing these data is to directly plot the energy barriers as a function of Φ_{eff} for a given film thickness, for example, $d = 10\,nm$ as indicated by the vertical line in Fig. 3b.

The obtained functional dependence (open symbols in Fig. 3c) is characterized by a slope of zero ($S = 0$) for low Φ_{eff}, a region with $S = 1$ for intermediate Φ_{eff}, and again $S = 0$ for high Φ_{eff}. The transitions between the different regions are marked by the so-called pinning work functions, $\Phi^- = 3.0\,eV$ for LUMO and $\Phi^+ = 4.4\,eV$ for HOMO pinning with the latter matching the experimental value for a 10-nm film of pentacene[36]. The term pinning refers to the observation that, for multilayer organic semiconductor films of device-relevant thickness, E_F cannot cross the HOMO or LUMO level onsets (marked as horizontal lines) and, thus, energy barriers/losses cannot be completely eliminated; regardless of the choice for Φ_{eff}, the Fermi level appears to be 'stuck' at specific energy separations ($\sim 0.4\,eV$ for $d = 10\,nm$) well above/below the respective peak onsets.

In the past, this observation has led to the postulation of material-specific, discrete, quantum-mechanical states at these energies, the so-called 'integer charge-transfer' (ICT) states, with ICT^+ shifted up in energy from the HOMO onset and ICT^- shifted down in energy from the LUMO onset into the gap of the organic semiconductor[29]. As already pointed out in refs 25,27,28, however, the fact that the pinning energies of E_F in the organic semiconductor gap emerge naturally (and quantitatively correct) from electrostatics alone: (i) lifts the necessity for invoking the existence of such states and (ii) invalidates the interpretation of their energy separation from the HOMO and LUMO onsets as the respective polaron-binding energies λ^+ and λ^-. We explicitly illustrate this latter point in Fig. 3c for our Gaussian DOS (cf. ref. 28). For our considered model case, pentacene, the polaron-binding energy, that is, the energy stabilization of an

excess charge in the organic semiconductor by geometric relaxation of the charged molecule itself (internal relaxation energy) and of the surrounding lattice (external relaxation energy), was found to be only $\lambda^{+/-} = 0.07\,eV$ (refs 57,58) with the latter being negligible compared with the former[59]. This value is taken into account in equation (1) by shifting the HOMO and LUMO levels symmetrically towards each other, thus effectively reducing the gap of the organic semiconductor. The magnitude of the resulting changes (closed symbols in Fig. 3c) is, not unexpectedly, comparable to the absolute value of $\lambda^{+/-}$ and, thus, its contribution to the observed minimum barriers is smaller than the typical experimental accuracy of $\sim 0.1\,eV$; polaronic effects will, therefore, no longer be considered in the following.

Film thickness and Gaussian DOS. Briefly returning to Fig. 3b, it is evident that the relationship between $\Delta_{e/h}$ and Φ_{eff} changes with the total thickness of the organic film. In Fig. 4a, we show vertical cuts through the data presented in Fig. 3b not only for $d = 10\,nm$, as discussed in Fig. 3c, but for an entire series of thicknesses. As a direct consequence of band bending within the organic film, the substrate work functions where LUMO/HOMO pinning sets in successively decrease/increase with decreasing film thickness down to $\Phi^- = \sim 2.4\,eV$ and $\Phi^+ = \sim 4.7\,eV$, respectively, for a monolayer of pentacene, which, again, compares favourably to experiment[35]. Evidently, the thinner the organic semiconductor film, the lower Δ_e and Δ_h can be made by, respectively, decreasing or increasing Φ_{eff} until, in the extreme case of a monolayer, they vanish for $\Phi_{eff} = 5.5\,eV$ and $\Phi_{eff} = 1.8\,eV$, respectively (cf. refs 30–33).

The same could, arguably, be achieved also for thicker layers if the DOS tailing into the gap of the organic could be eliminated; it is the presence and the occupation of these gap states, after all, that prevents E_F from further approaching the HOMO/LUMO onsets. The origin of the gap states is commonly attributed to structural imperfection/defects[28,42,60–62]. Their density and energy distribution can experimentally be determined only on a case-by-case basis[60–62], as they depend on specifics of sample preparation and environment, that is, exact film structure and composition[60]. To elucidate their impact on energy level alignment on more general grounds, we vary the width of the HOMO- and LUMO-related DOS while keeping it Gaussian-shaped, which has been shown to phenomenologically emulate also the impact of exponential tails[27]. Leaving, at the same time, the energies of the peak maxima, E_H and E_L, unchanged, trivially leads to the HOMO and LUMO onsets moving into the gap and, consequently, to E_F getting pinned ever farther in the gap as well
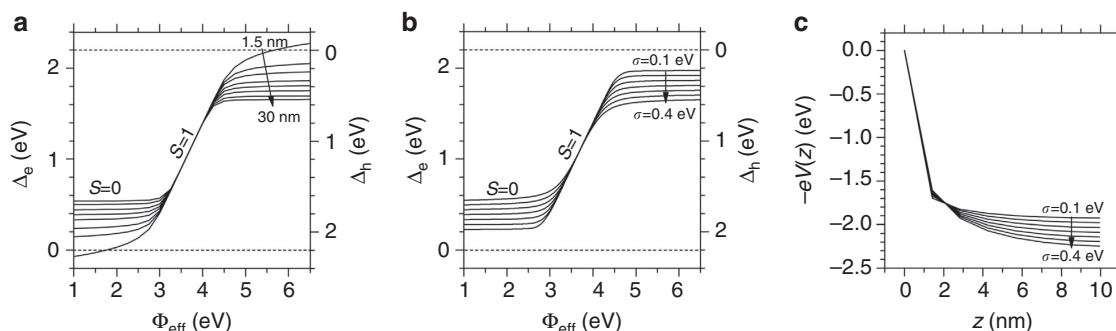
Figure 4 | Impact of film thickness and width of Gaussian DOS. (**a**) Injection barriers Δ_e for electrons (left axis) and Δ_h for hole (right axis) as a function of effective substrate work function Φ_{eff} for pentacene films of thicknesses from $d = 1.5\,nm$ to 30 nm. (**b**) Injection barriers Δ_e (left axis) and Δ_h (right axis) as a function of Φ_{eff} for a $d = 10\,nm$ thick pentacene film with the standard deviations of the Gaussian HOMO and LUMO DOS varied from $\sigma_{H/L} = 0.1\,eV$ up to $\sigma_{H/L} = 0.4\,eV$ while retaining a constant IE and EA. (**c**) Electron potential energy profiles $-eV(z)$ at the highest effective substrate work function $\Phi_{eff} = 6.5\,eV$ for all $\sigma_{H/L}$ treated in **b**.

(not shown). A maybe less trivial result is presented in Fig. 4b. There, we keep the HOMO and LUMO onsets, which represent the physical material parameters IE and EA, respectively, at constant energy. Varying the width of the DOS then requires adjusting the energy separation between the peak maxima accordingly. Even under these conditions, however, reducing the Gaussian width of HOMO- and LUMO-related DOS leads to (i) the transition between the regimes of Fermi level pinning ($S = 0$) and the Schottky–Mott limit ($S = 1$) to become more abrupt, (ii) E_F successively approaching the respective onsets in the pinning regimes and (iii) the spatial extent of the band-bending region to be reduced, as evidenced in Fig. 4c. The range of minimal energy barriers (~ 0.2 eV to ~ 0.6 eV) emerging from our model spans the entire range of values observed in experiment[44,55], highlighting the decisive role of disorder in the organic semiconductor in determining interfacial energy level alignment[60]. Note also that, for $T > 0$ K, finite barriers remain even in the limiting case $\sigma_{H/L} \to 0$ of discrete molecular states, which is, in fact, the only case treated in refs 23,25.

From band bending to interface dipole. Notably, the phenomenology described so far, the characteristic shape in Figs 3c and 4 in particular, is only ever observed for 'weakly' interacting electrode–organic interfaces. There, either through surface contamination or by design, the organic semiconductor is electronically decoupled from the metallic states by a thin, wide-gap buffer layer, which, in following refs 27,28, we did not explicitly take into account so far. As shown in the Supplementary Discussion, even doing so does not alter the fact that the interfacial energy level alignment between organic semiconductor and metallic electrode always falls into one of three regimes, HOMO pinning, Schottky–Mott limit and LUMO pinning, characterized by slope parameters $S = d\Delta_e/d\Phi_{eff} = -d\Delta_h/d\Phi_{eff}$ of (close to) zero, one and again zero, respectively (cf. Supplementary Figure 1). If, however, the buffer layer is eliminated completely in experiments, which can be achieved by, for example, depositing the organic semiconductor directly onto atomically clean metal surfaces in ultrahigh vacuum, also fractional slope parameters between 0 and 1 are frequently observed[26,36,39,55,63]. Despite having explored a good portion of the parameter space available in our model, we failed to generate non-integer values of S so far, whereas they are readily (and often quantitatively correct) predicted by the 'induced density of interface states' model[26,39].

This is surprising insofar, as this model is, in essence, quite similar to ours. Besides typically treating only molecular monolayers and assuming the organic DOS to be constant around E_F for evaluating S, the main difference lies in the peak shape, which the authors take to be Lorentzian rather than Gaussian. This is entirely reasonable for the envisioned situation, where direct electronic coupling of the monolayer molecular levels to the metal leads to homogenous life-time broadening dominating over disorder-induced inhomogeneous (that is, Gaussian) broadening[60]. Having already elucidated the impact of the latter in Fig. 4b, we now choose a Voigt peak function with successively increasing Lorentzian weight to represent the DOS of the first organic layer, while retaining pure Gaussians for all subsequent layers. The Φ_{eff}-dependence of the resulting injection barriers into a $d = 10$ nm film of pentacene is shown in Fig. 5a, containing also the limiting, pure-Gaussian case already reported in Fig. 3c for comparison.

Clearly, with increasing weight of the Lorentzian contribution, ever lower/higher substrate work functions are required to reach the same barriers for electrons/holes. More importantly, however, the Φ_{eff}-region of non-vanishing slope parameter expands, where S itself decreases from unity to a value of 0.42 for a Lorentz dominated (75%), down to 0.35 for an exclusively Lorentzian DOS, which brackets the experimental observed values of 0.37 and 0.40 for pentacene[55,63].

This remarkable transition between phenomenologically distinct energy level alignment regimes is accompanied by profound changes in the electron potential energy profile $-eV(z)$ within the organic semiconductor film (Fig. 5b). On increasing the Lorentz weight in the first-layer DOS, the spatially extended band-bending region in the organic is successively compressed towards the immediate interface with the electrode until, in the case of a pure Lorentzian, it collapses into a potential energy step across only the very first molecular layer. The abruptness of this step, which is not a unique feature of the Lorentzian peak shape *per se* but simply a consequence of the (compared to the Gaussian) higher DOS around E_F, has led to it being assimilated into the interface dipole (as defined above) in the past. This can be justified by considering that the combined action of all interfacial effects reduces the work function that subsequently deposited molecules 'see' to, in our case, $\Phi_{eff} - eV(d) = 6.5$ eV $- 2.1$ eV $= 4.4$ eV, which is, again, the HOMO-pinning work function Φ^+ of pentacene. Therefore, no further charge transfer
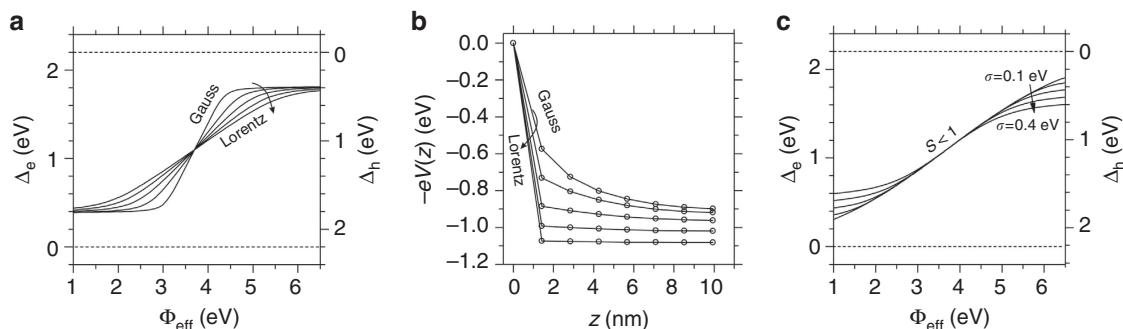
Figure 5 | Fractional slope parameters and band bending versus interface dipole. (a) Injection barriers Δ_e for electrons (left axis) and Δ_h for hole (right axis) as a function of effective substrate work function Φ_{eff} for a $d = 10$ nm pentacene film. The peak shape of the HOMO- and LUMO-derived DOS in the first layer is successively varied from pure Gaussian over Voigt to pure Lorentzian. **(b)** Electron potential energy $-eV(z)$ within a $d = 10$ nm pentacene film and a Φ_{eff} of 5.3 eV. Changing the peak shape of the HOMO- and LUMO-derived DOS in the first layer from pure Gaussian over Voigt to pure Lorentzian leads to a collapse of the spatially extended band-bending region to an interface dipole across the first molecular layer. **(c)** Injection barriers Δ_e for electrons (left axis) and Δ_h for holes (right axis) as a function of effective substrate work function Φ_{eff} for a $d = 10$ nm pentacene film. The DOS of the first layer is kept fixed to a Lorentzian peak shape of width 0.25 eV, whereas the standard deviations $\sigma_{H/L}$ of the Gaussian peak shapes in all subsequent layers increase from 0.1 eV up to 0.4 eV. Although the range of linearity decreases succeedingly, the value of the slope parameter S < 1 remains unchanged.

between the monolayer-covered electrode and succeeding organic semiconductor layers occurs and, with Δ_h having reached its minimum value of 0.4 eV already, no additional shifts in electron potential energy arise. Deviation from a strictly linear evolution of $\Delta_{h/e}$ is not observed until the Gaussian DOS of subsequent bulk layers again tails across E_F for extreme values of Φ_{eff}, thereby causing residual band bending. The range of linearity is thus restricted by the amount of energetic disorder in the bulk (exemplified by $\sigma_{H/L}$-values ranging from 0.1 eV up to 0.4 eV in Fig. 5c), but the absolute value of the slope parameter $S < 1$ is not affected. This noteworthy result rationalizes the success of the induced density of interface state model in correctly reproducing the interfacial energy level alignment in the limiting case of atomically clean metals with intermediate work functions, despite it considering only monolayer coverage.

Discussion

To summarize, we present the results of a single, versatile electrostatic model, from which all observed regimes of energy level alignment at metal/(insulator/)organic semiconductor interfaces emerge naturally. Although designed to accommodate unprecedented detail and complexity, it contains prior work as limiting cases, notably, that of Ley et al.[25], which is limited to producing either VL alignment ($S = 1$) or Fermi level pinning ($S = 0$) as a consequence of considering only discrete molecular states; that of Blakesley et al.[27,28], which does not explicitly include insulating buffer layers and, thus, overestimates interfacial charge densities, as shown in the Supplementary Discussion; and that of Vazquez et al.[26], which is limited to a single molecular layer with Lorentzian DOS and, thus, fails to predict band bending. In providing a unified picture of the underlying physical mechanisms, our model confirms that the DOS of the organic semiconductor is the central, decisive quantity, responsible for all experimentally encountered phenomena and that controlling it is, therefore, key to minimizing charge carrier injection barriers and/or extraction losses beyond what is possible by adjusting the electrode work function alone.

Using high (for holes) and low (for electrons) work-function electrodes is, of course, still a necessary prerequisite. Our results illustrate, however, that there are intrinsic limits to this strategy and that, to overcome these limits, the amount of electronic states in the energy gap of the organic semiconductor (as well as their energetic separation from its band edges) must be reduced. Besides eliminating defects within the organic semiconductor, our model suggests electronic decoupling from the metallic electrode to be a critical component in achieving this, thereby providing a theoretically well-founded justification for the wide-spread use of thin passivating buffer layers. As a further beneficial consequence of 'cleaning out the gap', spatially extended band-bending regions are predicted to develop within the organic semiconductor, which, in contrast to sharply localized interface dipoles, further lower effective injection barriers in OLEDs under applied bias voltage and facilitate the efficient collection of photo-generated charge carriers in OPVCs by imposing a drift direction. Our results thus provide a solid theoretical basis for past and present efforts in optimizing the interfacial energy level alignment at organic semiconductor/electrode contacts and will, hopefully, inspire future work.

References

1. Friend, R. H. et al. Electroluminescence in conjugated polymers. Nature 397, 121–128 (1999).
2. Walzer, K., Maennig, B., Pfeiffer, M. & Leo, K. Highly efficient organic devices based on electrically doped transport layers. Chem. Rev. 107, 1233–1271 (2007).
3. Meyer, J. et al. Transition Metal Oxides for Organic Electronics: Energetics, Device Physics and Applications. Adv. Mater. 24, 5408–5427 (2012).
4. Wong, W. Y. & Ho, C. L. Functional metallophosphors for effective charge carrier injection/transport: new robust OLED materials with emerging applications. J. Mater. Chem. 19, 4457–4482 (2009).
5. Sun, Y. R. et al. Management of singlet and triplet excitons for efficient white organic light-emitting devices. Nature 440, 908–912 (2006).
6. Burroughes, J. H. et al. Light-emitting-diodes based on conjugated polymers. Nature 347, 539–541 (1990).
7. Dodabalapur, A., Torsi, L. & Katz, H. E. Organic transistors: 2-dimensional transport and improved electrical characteristics. Science 268, 270–271 (1995).
8. Usta, H., Facchetti, A. & Marks, T. J. n-Channel semiconductor materials design for organic complementary circuits. Acc. Chem. Res. 44, 501–510 (2011).
9. Klauk, H., Zschieschang, U., Pflaum, J. & Halik, M. Ultralow-power organic complementary circuits. Nature 445, 745–748 (2007).
10. Braga, D. & Horowitz, G. High-performance organic field-effect transistors. Adv. Mater. 21, 1473–1486 (2009).
11. Dimitrakopoulos, C. D. & Malenfant, P. R. L. Organic thin film transistors for large area electronics. Adv. Mater. 14, 99–117 (2002).
12. Peumans, P., Uchida, S. & Forrest, S. R. Efficient bulk heterojunction photovoltaic cells using small-molecular-weight organic thin films. Nature 425, 158–162 (2003).
13. Gunes, S., Neugebauer, H. & Sariciftci, N. S. Conjugated polymer-based organic solar cells. Chem. Rev. 107, 1324–1338 (2007).
14. Heeger, A. J. Semiconducting and metallic polymers: The fourth generation of polymeric materials (Nobel lecture). Angew. Chem. Int. Edit 40, 2591–2611 (2001).
15. Kim, J. Y. et al. Efficient tandem polymer solar cells fabricated by all-solution processing. Science 317, 222–225 (2007).
16. Dennler, G., Scharber, M. C. & Brabec, C. J. Polymer-Fullerene Bulk-Heterojunction Solar Cells. Adv. Mater. 21, 1323–1338 (2009).
17. Steim, R., Kogler, F. R. & Brabec, C. J. Interface materials for organic solar cells. J. Mater. Chem. 20, 2499–2512 (2010).
18. Blom, P. W. M., Mihailetchi, V. D., Koster, L. J. A. & Markov, D. E. Device physics of polymer: fullerene bulk heterojunction solar cells. Adv. Mater. 19, 1551–1566 (2007).
19. Hwang, J., Wan, A. & Kahn, A. Energetics of metal-organic interfaces: new experiments and assessment of the field. Mater. Sci. Eng. R 64, 1–31 (2009).
20. Koch, N. Organic electronic devices and their functional interfaces. Chem. Phys. Chem 8, 1438–1455 (2007).
21. Ishii, H., Sugiyama, K., Ito, E. & Seki, K. Energy level alignment and interfacial electronic structures at organic metal and organic organic interfaces. Adv. Mater. 11, 605–625 (1999).
22. Ishii, H. & Seki, K. Energy level alignment at organic/metal interfaces studied by UV photoemission: breakdown of traditional assumption of a common vacuum level at the interface. IEEE T Electron Dev. 44, 1295–1301 (1997).
23. Greiner, M. T. et al. Universal energy-level alignment of molecules on metal oxides. Nat. Mater. 11, 76–81 (2012).
24. Wang, H. et al. Band-bending in organic semiconductors: the role of alkali-halide interlayers. Adv. Mater. 26, 925–930 (2014).
25. Ley, L., Smets, Y., Pakes, C. I. & Ristein, J. Calculating the universal energy-level alignment of organic molecules on metal oxides. Adv. Funct. Mater. 23, 794–805 (2013).
26. Vazquez, H., Flores, F. & Kahn, A. Induced density of states model for weakly-interacting organic semiconductor interfaces. Org. Electron. 8, 241–248 (2007).
27. Lange, I. et al. Band bending in conjugated polymer layers. Phys. Rev. Lett. 106, 216402 (2011).
28. Blakesley, J. C. & Greenham, N. C. Charge transfer at polymer-electrode interfaces: The effect of energetic disorder and thermal injection on band bending and open-circuit voltage. J. Appl. Phys. 106, 034507 (2009).
29. Braun, S., Salaneck, W. R. & Fahlman, M. Energy-Level Alignment at Organic/Metal and Organic/Organic Interfaces. Adv. Mater. 21, 1450–1472 (2009).
30. Berkebile, S. et al. A momentum space view of the surface chemical bond. Phys. Chem. Chem. Phys. 13, 3604–3611 (2011).
31. Puschnig, P. et al. Orbital tomography: deconvoluting photoemission spectra of organic molecules. Phys. Rev. B 84, 235427 (2011).
32. Wiessner, M. et al. Substrate-mediated band-dispersion of adsorbate molecular states. Nat. Commun. 4, 1514 (2013).
33. Oehzelt, M. et al. The molecular orientation of para-sexiphenyl on Cu(110) and Cu(110) p(2 × 1)O. Chem. Phys. Chem. 8, 1707–1712 (2007).
34. Heimel, G. et al. Charged and metallic molecular monolayers through surface-induced aromatic stabilization. Nat. Chem. 5, 187–194 (2013).
35. Fukagawa, H. et al. The role of the ionization potential in vacuum-level alignment at organic semiconductor interfaces. Adv. Mater. 19, 665–668 (2007).
36. Koch, N., Elschner, A., Rabe, J. P. & Johnson, R. L. Work function independent hole-injection barriers between pentacene and conducting polymers. Adv. Mater. 17, 330–335 (2005).

37. Knupfer, M. & Peisert, H. Electronic properties of interfaces between model organic semiconductors and metals. *Physica Status Solidi A* **201,** 1055–1074 (2004).

38. Koller, G. *et al.* The electronic band alignment on nanoscopically patterned substrates. *Org. Electron.* **8,** 63–68 (2007).

39. Vazquez, H. *et al.* Barrier formation at metal-organic interfaces: dipole formation and the charge neutrality level. *Appl. Surf. Sci.* **234,** 107–112 (2004).

40. Winkler, S. *et al.* The impact of local work function variations on fermi level pinning of organic semiconductors. *J. Phys. Chem. C* **117,** 22285–22289 (2013).

41. Niederhausen, J. *et al.* Doping of C-60 (sub)monolayers by Fermi-level pinning induced electron transfer. *Phys. Rev. B* **86,** 081411 (2012).

42. Sueyoshi, T., Fukagawa, H., Ono, M., Kera, S. & Ueno, N. Low-density band-gap states in pentacene thin films probed with ultrahigh-sensitivity ultraviolet photoelectron spectroscopy. *Appl. Phys. Lett.* **95,** 183303 (2009).

43. Bassler, H. Charge transport in disordered organic photoconductors—a monte carlo simulation study. *Physica Status Solidi B* **175,** 15–56 (1993).

44. Fukagawa, H. *et al.* Origin of the highest occupied band position in pentacene films from ultraviolet photoelectron spectroscopy: Hole stabilization versus band dispersion. *Phys. Rev. B* **73,** 245310 (2006).

45. Han, W. N., Yoshida, H., Ueno, N. & Kera, S. Electron affinity of pentacene thin film studied by radiation-damage free inverse photoemission spectroscopy. *Appl. Phys. Lett.* **103,** 123303 (2013).

46. Campbell, R. B., Robertson, J. M. & Trotter, J. The crystal structure of hexacene, and a revision of crystallographic data for tetracene and pentacene. *Acta. Crystallogr.* **15,** 289–290 (1962).

47. Kim, C. H. *et al.* Capacitive behavior of pentacene-based diodes: quasistatic dielectric constant and dielectric strength. *J. Appl. Phys.* **109,** 083710 (2011).

48. Ishii, H. *et al.* Kelvin probe study of band bending at organic semiconductor/metal interfaces: examination of Fermi level alignment. *Physica Status Solidi A* **201,** 1075–1094 (2004).

49. Chan, C. K., Kim, E. G., Bredas, J. L. & Kahn, A. Molecular n-type doping of 1,4,5,8-naphthalene tetracarboxylic dianhydride by pyronin B studied using direct and inverse photoelectron spectroscopies. *Adv. Funct. Mater.* **16,** 831–837 (2006).

50. Arch, J. K. & Fonash, S. J. Computer simulations of actual and Kelvin-probe-measured potential profiles: application to amorphous films. *J. Appl. Phys.* **68,** 591–600 (1990).

51. Simmons, J. G. Theory of metallic contacts on high resistivity solids - I. Shallow traps. *J. Phys. Chem. Solids* **32,** 1987–1999 (1971).

52. Simmons, J. G. Theory of metallic contacts on high resistivity solids (II) deep traps. *J Phys. Chem. Solids* **32,** 2581–2591 (1971).

53. Ottinger, O. M., Melzer, C. & von Seggern, H. Pitfalls in Kelvin probe measurements. *J. Appl. Phys.* **106,** 023704 (2009).

54. Ishii, H. *et al.* The electronic structure and energy level alignment of porphyrin/metal interfaces studied by ultraviolet photoelectron spectroscopy. *J. Electron. Spectrosc.* **76,** 559–564 (1995).

55. Koch, N. & Vollmer, A. Electrode-molecular semiconductor contacts: Work-function-dependent hole injection barriers versus Fermi-level pinning. *Appl. Phys. Lett.* **89,** 162107 (2006).

56. Toader, M., Shukrynau, P., Knupfer, M., Zahn, D. R. T. & Hietschold, M. Site-Dependent Donation/Backdonation Charge Transfer at the CoPc/Ag(111) Interface. *Langmuir* **28,** 13325–13330 (2012).

57. Coropceanu, V. *et al.* Hole- and electron-vibrational couplings in oligoacene crystals: Intramolecular contributions. *Phys. Rev. Lett.* **89,** 275503 (2002).

58. Norton, J. E. & Bredas, J. L. Polarization energies in oligoacene semiconductor crystals. *J. Am. Chem. Soc.* **130,** 12377–12384 (2008).

59. McMahon, D. P. & Troisi, A. Evaluation of the External Reorganization Energy of Polyacenes. *J. Phys. Chem. Lett.* **1,** 941–946 (2010).

60. Bussolotti, F., Kera, S., Kudo, K., Kahn, A. & Ueno, N. Gap states in pentacene thin film induced by inert gas exposure. *Phys. Rev. Lett.* **110,** 267602 (2013).

61. Kalb, W. L. & Batlogg, B. Calculating the trap density of states in organic field-effect transistors from experiment: a comparison of different methods. *Phys. Rev. B* **81,** 035327 (2010).

62. Yogev, S. *et al.* Fermi level pinning by gap states in organic semiconductors. *Phys. Rev. Lett.* **110,** 036803 (2013).

63. Jaeckel, B., Sambur, J. B. & Parkinson, B. A. The influence of metal work function on the barrier heights of metal/pentacene junctions. *J. Appl. Phys.* **103,** 063719 (2008).

Author contributions

M.O. and G.H. devised the model and co-wrote the paper. M.O. implemented the model and performed all calculations. N.K. contributed to content discussions and the writing of the paper.

Additional information

Supplementary Information accompanies this paper at http://www.nature.com/naturecommunications

Competing financial interests: The authors declare no competing financial interests.

Reprints and permission information is available online at http://npg.nature.com/reprintsandpermissions/

How to cite this article: Oehzelt, M. *et al.* Organic semiconductor density of states controls the energy level alignment at electrode interfaces. *Nat. Commun.* 5:4174 doi: 10.1038/ncomms5174 (2014).